DESIGN, MANUFACTURING, AND TESTING OF 3D PRINTED COMPLIANT MECHANISMS FOR LUNAR EQUIPMENT

Dorota Budzyń [(1)], Aidan Cowley [(2)], Maciej Ossowski [(4)], Michał Siemaszko [(5)], Hossein Zare-Behtash [(5)], Andrea Cammarano [(6)]

[(1)] University of Glasgow, Glasgow, Scotland, G12 8QQ, United Kingdom, d.budzyn.1@research.gla.ac.uk
[(2)] European Space Agency, European Astronaut Centre, Linder Höhe, Cologne 51147, Germany, aidan.cowley@esa.int
[(4)] Astronika, Bartycka 18, 00-716 Warszawa, Poland, mossowski@astronika.pl
[(5)] Zortrax, Lubelska 34, 10-409 Olsztyn, Poland, michał.siemaszko@zortrax.com
[(5)] University of Glasgow, Glasgow, Scotland, G12 8QQ, United Kingdom, hossein.zare-behtash@glasgow.ac.uk
[(6)] University of Glasgow, Glasgow, Scotland, G12 8QQ, United Kingdom, andrea.cammarano@glasgow.ac.uk

1 ABSTRACT

Lunar regolith consists of varying grain sizes, including the very fine lunar dust that negatively impacts exploration hardware by jamming mechanisms and increasing friction. To address this issue, we propose the use of compliant mechanisms that rely on elastic deformation to achieve motion without the use of inter-element gaps. Such mechanisms are also an outstanding choice for applications requiring precision and avoiding lubrication and surface wear debris. Our design approach involves topology optimisation and analytical redesign to minimize stress. In this work we present a gripper design, 3D-printed with space-grade PEEK, and we share results of force and displacement tests, along with key lessons learned. Our methodology can guide future designs and be applied to a range of materials and space applications.

2 COMPLIANT MECHANISMS FOR IMPLICIT LUNAR DUST MITIGATION

Lunar dust is a mixture of rock fragments, minerals, glass, and glass aggregates. Due to its abrasive properties and the potential for it to enter gaps between equipment components, the dust poses a challenge to hardware used on the Moon [1, 2]. Lunar dust particles have sharp and serrated edges and can float above the surface in a levitation-like manner due to the electrostatic charge build-up on the surface of the Moon [3, 4]. This phenomenon can make it challenging to keep equipment away from the dust and can cause contamination. Additionally, dust ejected from the surface by any robotic or human activity stays above the surface for longer and can travel further due to the lack of atmosphere and reduced gravity.

The Apollo missions were initiated to accomplish various objectives such as performing crewed lunar landings, collecting lunar samples, evaluating landing capabilities, and assessing the capabilities of astronauts and their equipment in the lunar environment. Specific scientific experiments, including lunar dust detectors, lunar ejecta, and micrometeorites experiment, and charged particle lunar environment experiment, were developed to collect data from the Moon [5].

The lunar dust posed several challenges to the astronauts and hardware, such as clogging of mechanisms, abrasion, dust coating, inhalation and irritation among others [2, 6]. The wide range of problems caused by the lunar dust suggests that a variety of mitigation methods involving multiple technologies may be necessary [7]. The work presented in this paper focuses on the issues of clogged lunar mechanisms and proposes usage of gap-free mechanisms that are naturally dust resilient to dust induced jamming – namely compliant mechanisms.

Compliant mechanisms possess the remarkable capability to achieve motion without relying on numerous components or necessitating lubrication for inter-element movement. This feat is accomplished through elastic deformation. Furthermore, compliant mechanisms inherently serve as a dust mitigation technology since they eliminate inter-element gaps, thereby minimising the risk of jamming due to lunar dust particles intrusions. Compliant mechanisms demonstrate significant advantages in sustaining long-term hardware performance in environments where frictionless solutions are desired, such as the lunar surface, where regolith dust can cause mechanical wear and damage.

In recent years compliant mechanisms have gained popularity for space applications. Their lack of backlashes between the moving elements can improve positioning accuracy (especially for small displacements), furthermore, as it is tribology-free technology the lack of lubricants can be advantageous for mechanisms located in proximity of optical instruments that are usually sensitive to lubrication debris contamination. Additionally, compliant mechanisms can be manufactured more efficiently at small scales and require no assembly, making them ideal for use in micro-electro-mechanical systems (MEMS) [8–10]. Compliant mechanisms are also mass and volume saving substitutes for spring loaded mechanisms, as they store elastic energy that can be used to deploy appendages. In fact, tape spring hinges are standard solutions for deployment. While our focus in this study revolves around advocating the utilization of compliant mechanisms for managing

the risk of dust damage on the Moon, it is crucial to acknowledge that the benefits of such mechanisms extend beyond this specific application. The advantages attributed to compliant mechanisms render them highly valuable for a diverse array of space missions. Consequently, we firmly assert that the advantages outlined here establish the importance of developing compliant mechanisms for space exploration.

3 CASE STUDY: COMPLIANT GRIPPER

The compliant gripper developed in this project was inspired by the Apollo geological tool depicted in figure 1. The Tongs were employed to grip rock samples ranging in size up to 10 cm [11]. Due to the stiffness of the Apollo spacesuits, astronauts lacked the necessary dexterity to easily kneel and collect rocks with their hands. Tongs were therefore employed as an alternative method to retrieve rocks without requiring the astronauts to kneel or bend over.

Figure 1. The training replica of Apollo Tongs photographed in ESA EAC [12].

While the Tongs mechanism relies on spring-loading for jaw movement, the new compliant design explores alternative approach to use a compliant gripper. By utilising elastic deformation, the new design eliminates the need for a spring and achieves motion through elastic deformation. The gripper system design is displacement-driven, meaning that the position of the input handle directly determines the position of the output jaws. For the new compliant design, the default position of the gripper is assumed to be open with the ability of closing with input displacement pushing on the input port. The kinematic behaviour of the gripper is demonstrated in figure 2.

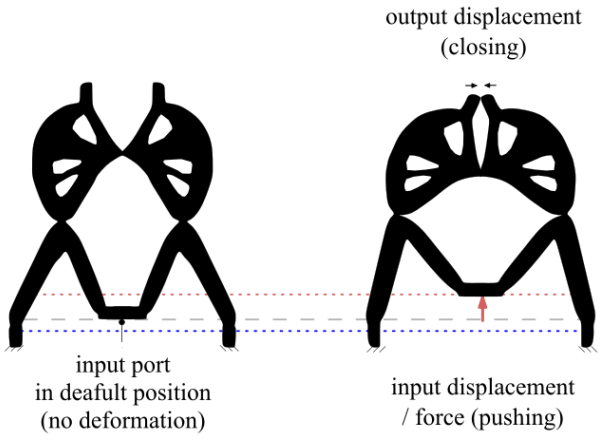

Figure 2. Expected kinematic behaviour of complaint gripper: left - default gripper position, right - pushing on the input port to close the gripper.

To ensure efficient transfer of input energy to output displacement, the jaw closing action should be achieved through horizontal displacement of the jaws, with minimal vertical movement. Most compliant designs are easily scalable and can be adjusted for larger or smaller gripping tasks. In this project, the objective was to develop a gripper capable of grasping elements up to 4 cm, while the Tongs could grasp samples up to 10 cm. The designs presented in the following section can be scaled accordingly for specific gripping tasks. Furthermore, the methodology used here can be easily adopted to other complaint designs.

4 DESIGN

Multiple design methodologies exist to synthesize a compliant mechanism. The discussion on different approaches, their advantages and limitations are outside of the scope of this paper. The design presented here was achieved using topology optimization which requires specification of some boundary conditions, one of which is the material. Polyetheretherketone (PEEK), selected for this project, is a high-performance polymer that offers several advantages including its lightweight nature, high strength and stiffness, thermal stability, radiation resistance, chemical resistance, low outgassing, and electrical insulation properties.
The next section focuses on the design process that was performed with PEEK material properties in the topology optimization process.

4.1 Topology optimisation

Topology optimization is a computational design technique that aims to optimize the material distribution for a given problem described by optimisation objective and constraints. In structural topology optimisation often, the objective is maximisation of a stiffness for given mass, or minimization of mass for given minimum stiffness. It involves iteratively removing unnecessary material while maintaining structural integrity. By maximising the efficiency of material usage, topology optimization can result in lightweight and structurally optimized designs with improved desired properties. Compliant mechanism design with the use of topology optimisation poses a challenge because of the difficulty with formulation of the objective function. Discussion on this topic is well covered in the literature [13]. To ease the formulation effort a novel topology optimisation design approach - *A simple and versatile topology optimization formulation for flexure design* – was introduced by Koppen [14]. Here, this methodology was utilised as a starting point for the design. The method of Koppen [14] was developed for small stroke flexures but can also be used to design more complex compliant mechanisms. It utilises two load cases with prescribed displacements. In displacement driven topology optimisation, compliance and stiffness are proportional. This is the different in load driven conditions where

compliance is inverse of stiffness. More details about the implications of these differences can be found in the literature [12,15,16]. The two mentioned displacement driven load cases are presented in table 1 with the design domain and position of input displacement (d_{in}) and output displacement (d_{out}) provided in figure 3.

Table 1. Values of prescribed displacements, design objective and constraints presented for two loading conditions.

	Load case	
	I	II
Input d_{in}	+ 1	+ 1
Output d_{out}	+ 1	- 1
Objective	-	maximize compliance
Constraints	compliance ≤ 0.1 Nmm	-
	volume fraction ≤ 0.4	
	stress constraint ≤ 70 MPa	

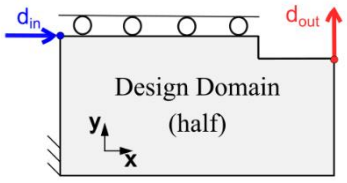

Figure 3. Design domain (half) of compliant gripper with input and output displacements marked.

The first load case represents the desired deflection of the gripper, while in the second load case, the output displacement has direction opposite to desired movement. As such the stiffness needs to be maximized for the second load case, and as already mentioned, for prescribed displacements this is equivalent to maximising compliance, which is indicated in the table. The first load case has maximum allowable compliance (proportional to stiffness) to ensure enough flexibility to achieve the displacements through deformation. Additionally, stress constraint was added to avoid so called point-hinges and volume constrained was added to drive the final volume of the mechanism. These load cases were modelled in the HyperWorks software together with constraints, objective and design parameters presented in the table 1. Moreover, the maximum iteration number set for this analysis was 500 and the material parameters of PEEK were modelled as follows: Young's modulus 3.72 GPa, Poisson ratio 0.38. The optimisation finished after 449 iterations. Selected topologies achieved throughout the topology optimisation process are presented in figure 4. To achieve the final design, finite elements with densities below 0.3 were removed from the design domain. In the next deign step, the final topology was mirrored to achieve full gripper design. Additionally, jaws and mounting holes were added to the model resulting in the final design presented in the figure 5a.

4.2 Analytical re-design step

The Finite Element Analysis (FEA), which is presented in figure 5b, was done to examine stress levels in the gripper with an input displacement large enough to close the jaws of the gripper. The Yield strength of PEEK was assumed to be 100 MPa, and as visible it was exceeded. This is why an analytical re-design step was also conducted aiming at minimising stress in the flexures. A simple mthod of allowing more deformation at lower stress is to extend the length of a flexure, which was done in this case as presented in figure 5c. FEA was conducted again with the use of the new model (see figure 5d), revealing a maximum stress of 54 MPa, which is a considerable improvement compared to the previous design. As such, topology optimisation found the general topology and positions of flexures while the analytical re-design step aimed at improving the flexures performance.

5 FABRICATION

PEEK was selected as the material for the gripper in this project due to its exceptional properties, including mechanical strength, low outgassing, and compatibility with 3D printing technologies. Manufacturing using 3D printing offers the possibility to produce complex and lightweight elements, such as compliant mechanisms. This has made additive manufacturing appealing for space, such that even the ISS, presently, features an Additive Manufacturing Facility. The hight melting temperature of PEEK also enhances its suitability for space application.

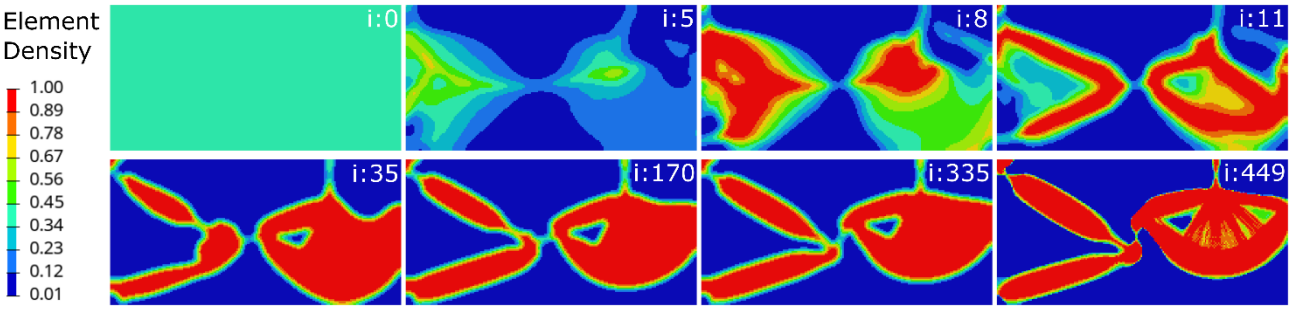

Figure 4. Evolution of topology optimisation with element densities marked; 'i' – iteration number.

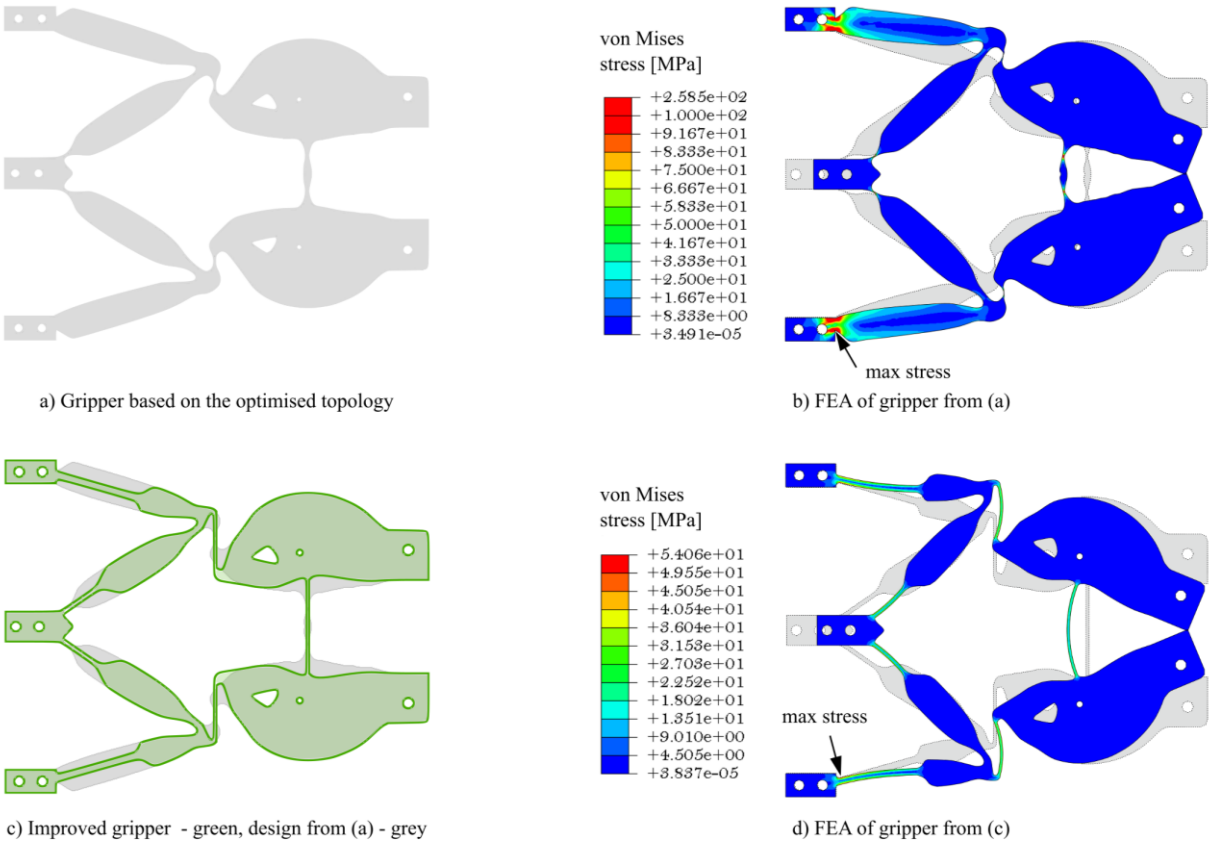

Figure 5. Various design steps undertaken to produce compliant PEEK gripper.

5.1 3D printing

The prints were produced using a Zortrax Endureal printer, utilising Z-PEEK as the printing material. The aim was to print in amorphous form which also allows the utilization of a second material - Z-Support ATP 130. To account for material shrinkage during printing and thermal post-processing (annealing), the prints were appropriately scaled to 102.4% in the XY axis and 101% in the Z axis. Depending on the model's geometry, scaling between 102% to 105% (XY) and 100.5% to 102% (Z) is commonly employed. As previously mentioned, the printing process took place in amorphous form, with an extrusion temperature of 400°C, a build plate temperature of 120°C, and a chamber temperature of 120°C. The dual extrusion mode was used, incorporating Z-Support ATP 130 as the support material. The typical supports were not necessary (as there were no overhanging parts), however utilising support material for the raft enhanced its easier removal in post processing of the specimen. Two grippers were printed (visible in Figure 6 one of which was left as is (in amorphous form) and another one was further thermally postprocessed to achieve semi-crystalline structure.

5.2 Annealing

Printing PEEK in amorphous form offers the opportunity to enhance detail printing control and improve the mechanical properties of the end-product while leaving room for thermal postprocessing - annealing - to achieve a semi-crystalline structure. During annealing, PEEK is subjected to a carefully controlled heat treatment to induce molecular reorganization and reduce internal stresses. The process involves heating the material above its glass transition temperature, allowing the amorphous regions of PEEK to become more ordered and crystalline in structure. This transition from the amorphous to the crystalline (or semi-crystalline) phase leads to improved mechanical properties, such as increased stiffness and strength, as well as enhanced dimensional stability.

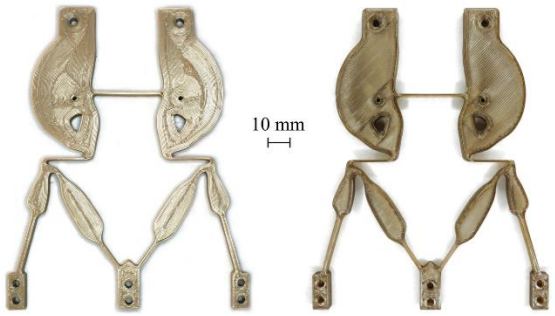

Figure 6. PEEK 3D printed grippers: annealed on the left and amorphous on the right.

Zortrax employs a specific annealing process involving placing the amorphous PEEK print in a sand-filled steel

container, which ensures superior thermal control and prevents model deformation. The quartz sand (0.2-0.8 mm grain gradation) surrounding the print decreases thermal inertia, providing mechanical stabilization, and minimises the risk of distortion. The annealing is conducted in a laboratory dryer, following a precise program: 3 hours at 100°C, followed by a gradual 3-hour temperature increase to 200°C (0.5 degrees per minute), 5 hours at 200°C, and finally, allowing natural cooling to room temperature.

6 TESTING

The afromentioned grippers (unannealed/amorphous and annealed/semi-crystalline) were subject to tests described in this section. The data presented here was obtained from two types of tests:

- Test 1: assessing the relationship between input and output displacements (input displacement applied and controlled by a mechanism with micrometre screw, output displacement determined by Digital Image Correlation - DIC);
- Test 2: assessing the relationship between input force and output displacement (input displacement applied with force gauge, output displacement determined by DIC).

Both tests were performed on two grippers: unannealed and annealed one. Furthermore, each test was repeated three times in a chamber with lunar regolith simulant EAC-1A and three times without it. This will be visible in the charts presented where test data without regolith is marked in green and the data achieved in the regolith simulant test is presented in red and blue (red for pushing on the input port and blue for retracting back/pulling).
The focus of the measurements was the output port which is the tip of the left jaw of the gripper (marked with blue coordinate system in figure 7). Nonetheless, because DIC was used in the measurements, the deformation of the whole gripper was also obtained, and will be presented. The DIC was conducted using the Matlab tool Ncorr [17]. In order to track displacements on the surface of the gripper a speckle pattern was applied. Furthermore, the test rig was equipped with a ruler to scale the deformations during the post processing. To ensure shift elimination between frames a calibration patch was used as visible in figure 7.

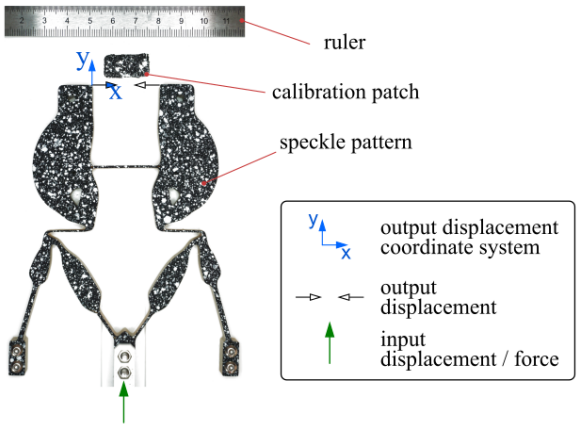

Figure 7. Gripper with speckle pattern (for DIC), mounted in the test rig.

Figure 8 presents the relationship between input and output displacements for the unannealed (a) and annealed (b) gripper. For both grippers the difference between tests carried out with and without the presence of regolith is negligible. Regardless of having the same geometry, as expected, both grippers have different stiffnesses which is visible in the input force difference required to close the jaws: 16.5 N for unannealed gripper and 26 for annealed gripper. This is caused by the difference in crystallinity levels in both grippers. The unannealed gripper requires less input displacement to fully close the jaws. Furthermore, linear regression of relationships between input and output displacement is a measure of

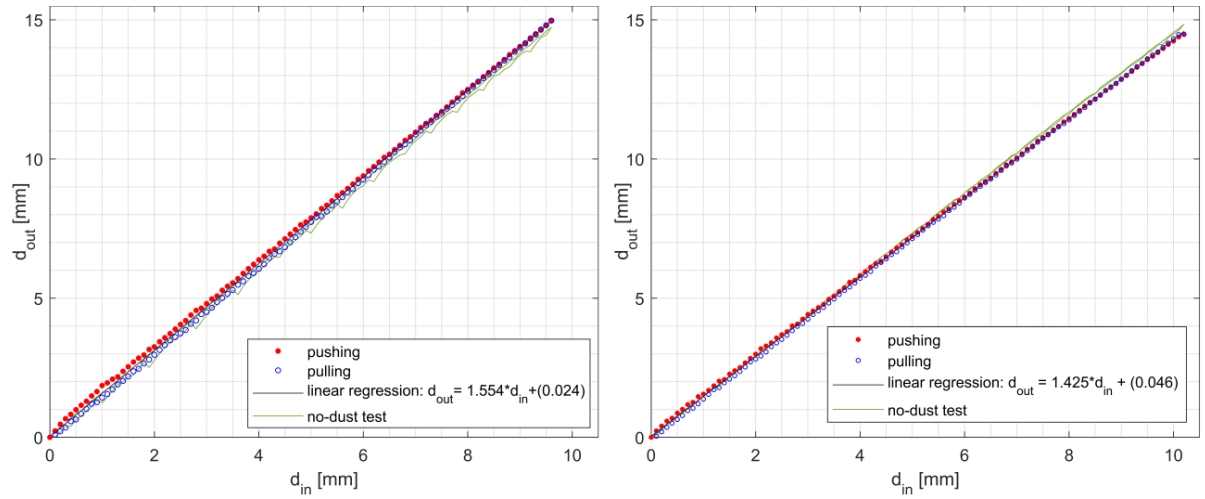

(a) unannealed gripper: input displacement - output displacement (horizontal) relationship

(b) annealed gripper: input displacement - output displacement (horizontal) relationship

Figure 8. Input displacement – output displacement test data: displacements relationship.

Geometric Advantage (GA) and, as visible, the GA of the unannealed gripper is higher. This implies that the annealed gripper requires more work to be elastically deformed.

Figure 7 presents the motion path of the output for both grippers. It can be seen that both paths are very similar, however the comparison between the test with and without regolith shows a small disturbance that is attributed to the interaction of the bottom surface of the gripper with the regolith filled test rig. Despite this additional friction, both grippers closed successfully.

Figure 8 takes a closer look at the GA calculated for each position of the gripper (all tests were done with 0.1 mm of input interval). It is important to note that the GA value of such compliant mechanisms changes, and the linear regression cannot fully capture the GA going from one position of the mechanism to another. The theoretical value of GA for both grippers is equal to 1. This is an outcome of using unit displacements (a value of 1 or -1) as prescribed displacements ($d_{in}/d_{out} = 1$) in the topology optimisation. As visible in the figure, the actual GA tested is much higher that the theoretical value of 1, but it is also important to note that the topology optimisation utilised here uses a linear analysis while the tests exceed the linear range of deformation. The difference between the GA for regolith and no regolith tests is negligible, meaning that in this case the dust interaction does not change the motion transmission in a significant manner.

The data from test 2 is provided in figure 9 which depicts the relationship between input force and output deformation. It can be seen that the annealed gripper is significantly stiffer as it requires more force to fully close. There is also a significant increase in the force needed to close the gripper in the regolith chamber: 1 N more for the unannealed and 2 N more for the annealed gripper. This is an effect of the regolith increasing friction between the gripper and test rig. However, as already demonstrated with test 1, the impact on the motion path and GA is negligible.

Finally, figure 10 presents DIC data to visualize the deformation of the gripper, the top row depicts the total displacement magnitude (absolute values) and the bottom row shows only the horizontal component of the displacement.

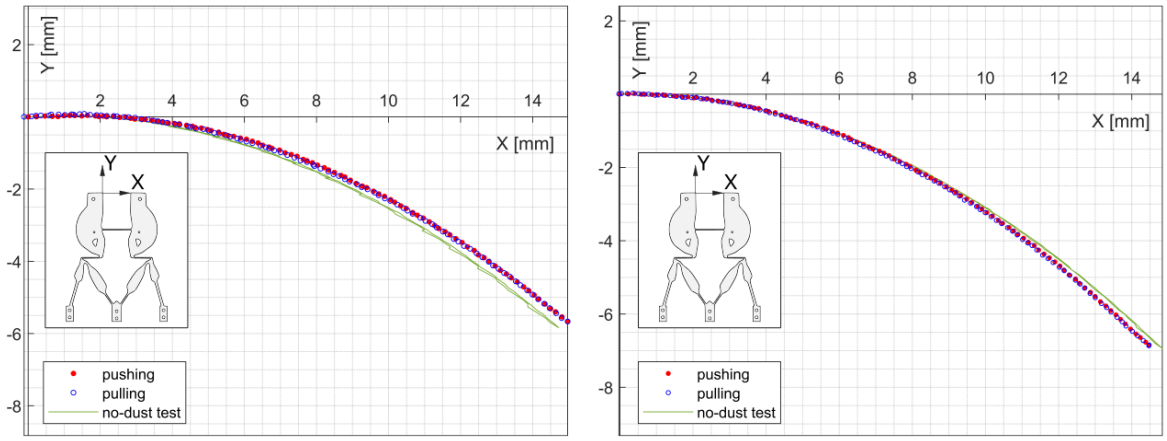

(a) unannealed gripper: output displacement path (b) annealed gripper: output displacement path

Figure 7. Input displacement – output displacement test data: output motion path.

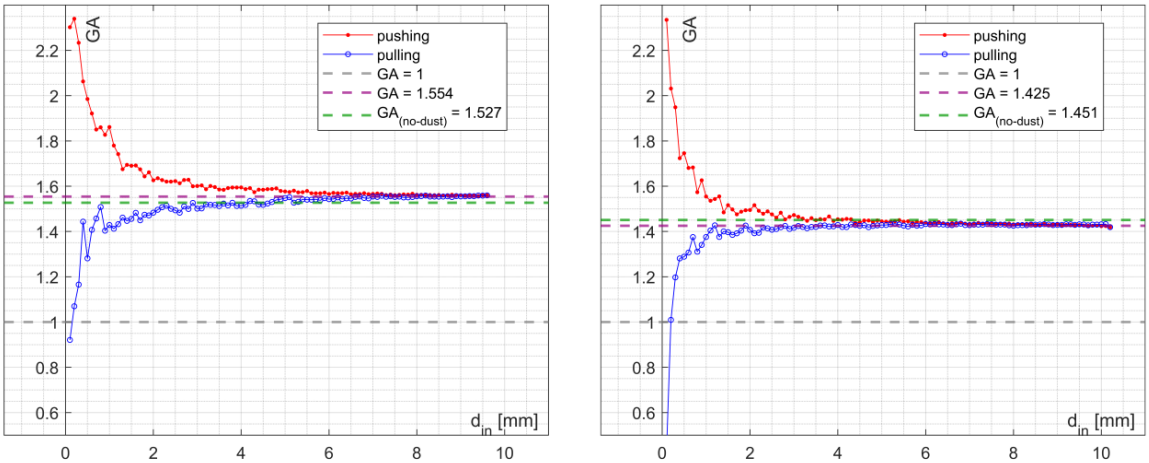

(a) unannealed gripper: input displacement - Geometric Advantage relationship (b) annealed gripper: input displacement - Geometric Advantage relationship

Figure 8. Input displacement – output displacement test data: GA changes.

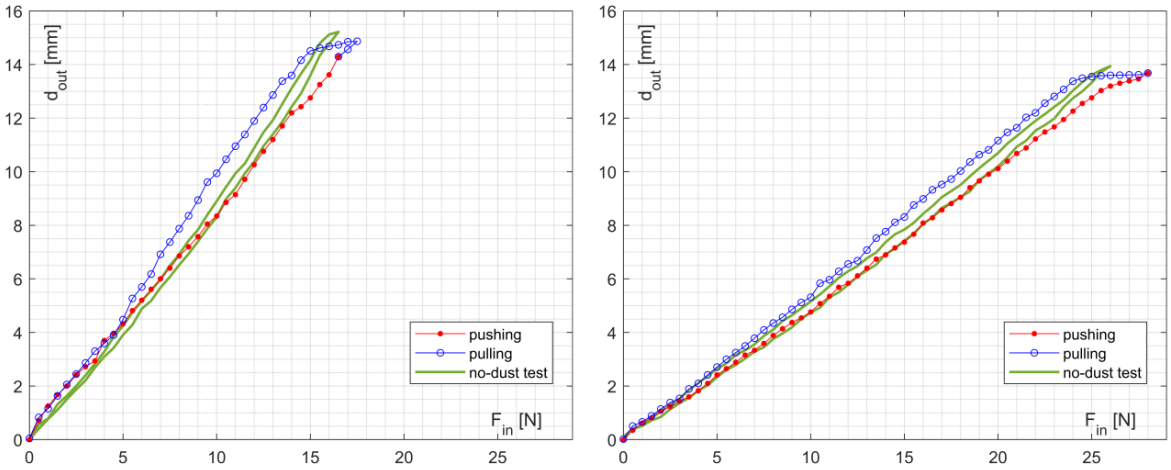

(a) unannealed gripper: input force - output displacement relationship

(b) annealed gripper: input force - output displacement relationship

Figure 9. Input force – output displacement test data: input force and output displacement relationship.

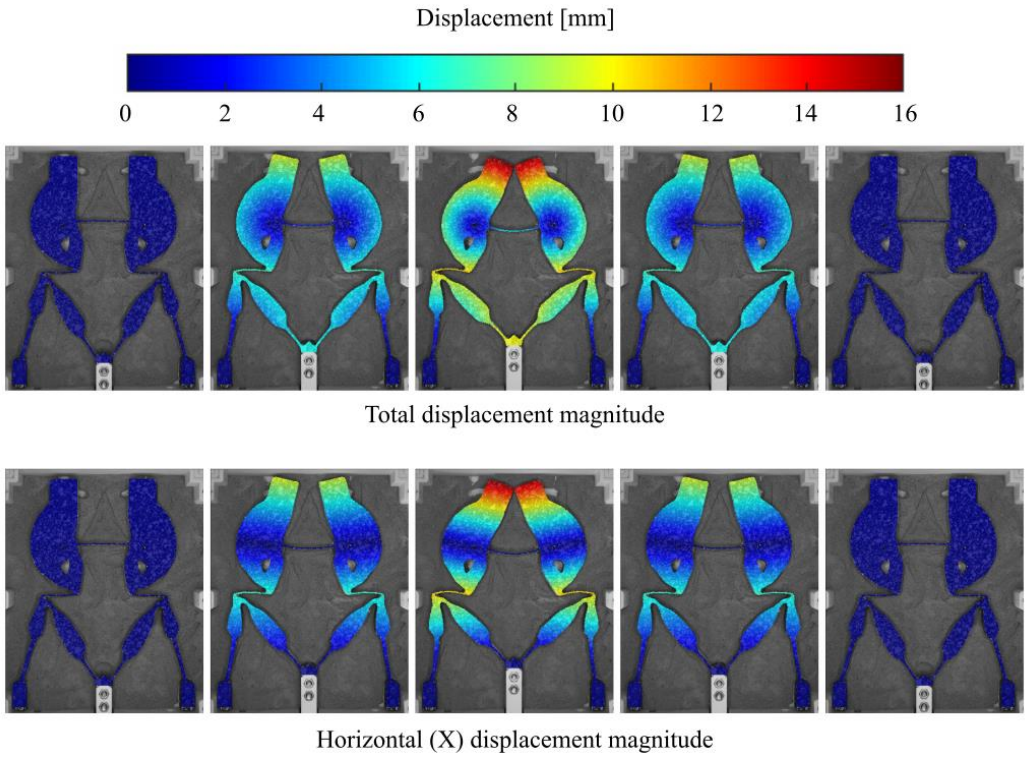

Figure 10. DIC data visualisation for annealed gripper tested in regolith simulant chamber – various deformation stages.

7 DISCUSSION AND FUTURE PROSPECTS

This paper presents the design and development of a compliant gripper. The gripper was designed to mimic the functionality of Apollo Tongs while exploring new design approaches using compliant mechanisms and novel topology optimisation formulation.

The tests clearly demonstrated the impact of heat treatment of PEEK on its elastic performance which is a crucial parameter for compliant mechanisms that must be considered while designing any compliant solution. The annealing increased the stiffness of the material, resulting in higher forces required to operate the gripper. But, as demonstrated, the kinematic behaviour remains unaltered. Furthermore, it has been demonstrated that complaint mechanisms do not change their motion path in the presence of dust, as expected for a tribology-free solution. However, as expected, dust intrusion can cause additional friction between compliant mechanisms and other equipment they are in contact with. As such, dust contamination should always be treated with caution. This work also demonstrated the convenience of using

DIC for assessment of complaint mechanisms deformation, which could also be used to enhance future designs by comparison of test DIC data with finite element analysis results.

It is important to recognize that 3D printed compliant mechanisms can undergo further modifications and improvements through additional treatments, which are not addressed in the research presented in this paper. However, some of these treatments are covered by the PEEK/Me project conducted by Astronika and Zortrax. The mentioned project investigates development of a new process for manufacturing PEEK-Metal composites which could help to further optimise the mechanical and surface properties of various PEEK parts including compliant mechanisms. The method combines 3D printing techniques with electroforming methods. The flexibility of 3D printing enhances production of sophisticated parts with a series of canals, which can become a structural reinforcement when filled through the deposition of metal. This could potentially enable various stiffness adjustment techniques enabling more flexibility in the design process of flexures. Examples of surface and structural metal reinforcement done on PEEK elements are presented in figure 11. In the future such postprocessing can help to build in metallic reinforcements into PEEK compliant mechanisms to enhance mechanical properties or improve the tribological contacts if required. More work in this area is expected to be undertaken by the authors of this paper.

Figure 11. 3D printed PEEK a) gears with and without additional metallic coating, b) PEEK/Me composite with applied metallic structural reinforcement and surface layer.

ACKNOWLEDGEMENTS

The University of Glasgow's project on compliant mechanisms for lunar environments is generously funded by the European Space Agency (ESA) through the ExPeRT (Exploration Preparation, Research, and Technology) program, grant number ESA AO/1-10811/21/NL/MG/idb. Additionally, the PEEK/Me project of Astronika, which focuses on the development of PEEK-Metal reinforced mechanical components for space applications and provided PEEK gripper samples, is funded by ESA under contract number 4000135312/21/NL/GLC/ov. The authors would like to express their sincere gratitude to ESA for the invaluable support in facilitating this research endeavour.

REFERENCES

[1] D. Budzyń *et al.*, "Lunar Dust: Its Impact on Hardware and Mitigation Technologies," *46th Aerospace Mechanisms Symposium*, p. 287, 2022.

[2] J. R. Gaier, "The Effects of Lunar Dust on EVA Systems During the Apollo Missions," *Nasa/Tm-2005-213610/Rev1*, no. March, pp. 1–16, 2007.

[3] J. E. Colwell, S. Batiste, M. Horányi, S. Robertson, and S. Sture, "Lunar surface: Dust dynamics and regolith mechanics," *Reviews of Geophysics*, vol. 45, no. 2, pp. 1–26, 2007.

[4] J. E. Colwell, S. R. Robertson, M. Horányi, X. Wang, A. Poppe, and P. Wheeler, "Lunar dust levitation," *J Aerosp Eng*, vol. 22, no. 1, pp. 2–9, 2009.

[5] Richard W. Orloff; David M. Harland, *Apollo: the definitive sourcebook*, vol. 44, no. 02. Springe, 2006.

[6] J. R. Gaier, "The Effects of Lunar Dust on EVA Systems During the Apollo Missions," *Nasa/Tm-2005-213610/Rev1*, no. March, 2007.

[7] S. Pirrotta, D. Lefebvre, M. W. Co-chair, H. Wong, J. Buffington, and J. J. Gaier, "DUST MITIGATION GAP ASSESSMENT REPORT," 2016.

[8] L. L. Howell, S. P. Magleby, and B. M. Olsen, *Handbook of Compliant Mechanisms*, no. 2013. 2013.

[9] R. M. Fowler, L. L. Howell, and S. P. Magleby, "Compliant space mechanisms: A new frontier for compliant mechanisms," *Mechanical Sciences*, vol. 2, no. 2, pp. 205–215, 2011.

[10] M. Kahr, H. Steiner, W. Hortschitz, M. Stifter, A. Kainz, and F. Keplinger, "3D-Printed MEMS Magnetometer Featuring Compliant Mechanism," *Proc West Mark Ed Assoc Conf*, vol. 2, no. 13, p. 784, 2018.

[11] J. H. Allton, "Catalog of Apollo Lunar Surface Geological Sampling Tools and Containers," 1989.

[12] D. Budzyń, H. Zare-behtash, A. Cowley, and A. Cammarano, "Implicit lunar dust mitigation technology: Compliant mechanisms," *Acta Astronaut*, vol. 203, no. September 2022, pp. 146–156, 2023.

[13] A. Saxena and G. K. Ananthasuresh, "On an optimal property of compliant topologies," *Structural and Multidisciplinary Optimization*, pp. 36–49, 2000.

[14] S. Koppen, M. Langelaar, and F. van Keulen, "A simple and versatile topology optimization formulation for flexure synthesis," *Mech Mach Theory*, vol. 172, no. January, p. 104743, 2022.

[15] A. Klarbring and N. Strömberg, "Topology optimization of hyperelastic bodies including non-zero prescribed displacements," *Structural and Multidisciplinary Optimization*, vol. 47, no. 1, 2013.

[16] F. Niu, S. Xu, and G. Cheng, "A general formulation of structural topology optimization for maximizing structural stiffness," *Structural and Multidisciplinary Optimization*, vol. 43, no. 4, pp. 561–572, 2011.

[17] J. Blaber, B. Adair, and A. Antoniou, "Ncorr: Open-Source 2D Digital Image Correlation Matlab Software," *Exp Mech*, vol. 55, no. 6, pp. 1105–1122, 2015.